© 2018. Published by The Company of Biologists Ltd.

Citron kinase-dependent F-actin maintenance at midbody secondary ingression sites mediates abscission.

Alessandro Dema[1,2], Francesca Macaluso[1], Francesco Sgrò[1], Gaia E. Berto[1,3], Federico T. Bianchi[1,3], Alessandra A. Chiotto[1,3], Gianmarco Pallavicini[1,3], Ferdinando Di Cunto[1,3,4*] and Marta Gai[1*].

[1]Dept. of Molecular Biotechnology and Health Sciences, University of Turin, Italy
[2]FMP-Berlin Campus Berlin-Buch, Robert-Roessle-Str. 10, 13125 Berlin, Germany
[3]Neuroscience Institute Cavalieri Ottolenghi, Turin, Italy
[4]Neuroscience Institute of Turin (NIT), Turin, Italy
* Corresponding Author. E-mail marta.gai@unito.it; ferdinando.dicunto@unito.it

Journal of Cell Science • Accepted manuscript

JCS Advance Online Article. Posted on 27 March 2018

Abstract

Abscission is the final step of cytokinesis whereby the intercellular bridge (ICB) linking the two daughter cells is cut. The ICB contains a structure called the midbody, required for the recruitment and organization of the abscission machinery. Final midbody severing is mediated by formation of secondary midbody ingression sites, where ESCRT III component CHMP4B is recruited and may mediate membrane fusion. It is presently unknown how cytoskeletal elements cooperate with CHMP4B to mediate abscission. In this report, we show that F-actin is associated with midbody secondary sites and is necessary for abscission. F-actin localization at secondary sites depends on the activity of RhoA and on the abscission regulator CITK. CITK depletion accelerates F-actin loss at the midbody and cytokinesis defects produced by CITK loss are reverted by restoring actin polymerization. Conversely, midbody hyperstabilization produced by CITK and ANLN overexpression is reverted by actin depolymerization. CITK is required for F-actin and ANLN localization at the abscission sites, as well as for CHMP4B recruitment. These results indicate that control of actin dynamics downstream of CITK prepares abscission site for final cut.

Journal of Cell Science • Accepted manuscript

Introduction

Cytokinesis is the terminal step of cell division leading to the physical separation of daughter cells. The actomyosin contractile machinery drives the ingression of the cleavage furrow (Eggert et al., 2006; Pollard, 2010). Actomyosin ring assembly and contraction are promoted by the small GTPase RhoA and its stabilization is regulated by ANLN, one of the crucial RhoA partners during cytokinesis (Piekny and Glotzer, 2008).

Furrow constriction allows the formation of a ICB containing bundles of antiparallel microtubules, which overlap at the midbody (Mierzwa and Gerlich, 2014). This structure provides a platform for the recruitment and organization of many proteins that regulate abscission (Agromayor and Martin-Serrano, 2013; Mierzwa and Gerlich, 2014).

After cleavage furrow ingression, the midbody is mechanically stabilized and anchored to the cell cortex by multiple mechanisms (Mierzwa and Gerlich, 2014). The ICB gradually narrows (Guizetti et al., 2011; Schiel et al., 2012) and two constriction zones, also called secondary ingression sites, form at both sides of the midbody (Elia et al., 2011; Guizetti et al., 2011; Schiel et al., 2011; Schiel et al., 2012).

The ESCRT-III complex, which is required to execute abscission, is first recruited to the midbody before relocalizing to constriction sites marking where the abscission occurs (Elia et al., 2011; Guizetti et al., 2011).

It is poorly understood how late midbody structures are organized. None of the microtubule-interacting proteins so far involved in cytokinesis has been found to localize in secondary ingression sites, whereas cleavage furrow proteins, such as ANLN and RhoA, localize not only to the furrow cortex and midbody, but also to constriction zones (Hu et al., 2012). It has been proposed that the ANLN–septin cytoskeleton primes the ICB for the recruitment of the ESCRT III subunit CHMP4B, leading to abscission (Renshaw et al., 2014). The localization of RhoA and ANLN at the midbody during late stages of cytokinesis depends on CITK, a protein required for spindle positioning (Gai et al., 2011) and abscission (Bassi et al., 2011; Bassi et al., 2013; El Amine et al., 2013; Gai et al., 2011; McKenzie et al., 2016; Watanabe et al., 2013). It has been demonstrated that CITK stabilizes midbody architecture by binding components of the contractile ring (ANLN, myosin and RhoA), central spindle (KIF23/MKLP1, KIF14) and the chromosomal passenger complex (Bassi et al., 2011; Bassi et al., 2013; Gai et al., 2011; Gruneberg et al., 2006; McKenzie et al., 2016; Watanabe et al., 2013). Moreover, CITK stabilizes midbody microtubules by increasing the phosphorylation of TUBB3 (Sgrò et al., 2015).

Journal of Cell Science • Accepted manuscript

These data suggest that CITK, together with ANLN and RhoA, could have a late role in cytokinesis, mediating ICB constriction and final cut.

In this report, we investigated whether the regulation of actin dynamics could control abscission by affecting constriction zones formation and maturation and addressed the possible role of CITK and its partner ANLN in this stage of cytokinesis.

Results and discussion

F-actin is required for normal abscission.

To start assessing the role of F-actin in abscission, we analyzed its organization in late midbodies, using super-resolution microscopy (Fig. 1A). Interestingly, we found that a small pool of F-actin localizes at secondary ingression sites (Fig. 1A,B,C), where it colocalizes with ANLN (Fig. 1D,F).

To address whether F-actin localization at secondary sites is necessary for ANLN localization, we treated synchronized HeLa with Cytochalasin D (CytoD). To avoid the detrimental effects of actin depolymerization on early cytokinesis stages, treatment was performed after complete cleavage furrow ingression, that is 120 minutes after nocodazole release. This treatment decreased F-actin localization at midbody, but did not alter significantly cell body fluorescence intensity (Fig. S1A). Especially, the frequency of secondary sites was not significantly different (Fig. S1B), but F-actin and ANLN were lost from these structures (Fig. 1D,E),

Next, to assess the role of RhoA on F-actin and ANLN localization in late midbody, we treated HeLa cells with the Rho inhibitor C3 transferase, upon complete furrow ingression. After this treatment, F-actin intensity decreased more in the midbody than in the cell body (Fig. S1C) and was not correctly distributed along the ICB: its accumulation was not centered on the secondary ingression sites (Fig. 1F,G). Even in this case, ANLN failed to localize at constriction sites (Fig. 1F,G).

Treatment of late cytokinesis cells with 0.4 μM or higher CytoD concentrations induced a significant increase in the number of binucleated cells (Fig. 1H). A similar effect was induced by RhoA inhibition through C3 treatment (Fig. 1I). To confirm that binucleation was due to cytokinesis failure after midbody formation, we observed by time-lapse microscopy control and treated cells in telophase at the time of drug addition (Fig. S1D, Movies 1,2). The number of cells that failed cytokinesis after cleavage ingression was

Journal of Cell Science • Accepted manuscript

significantly increased by CytoD treatment (Fig. S1E). Together, these results indicate that ANLN localization at secondary sites depends on the presence of F-actin at the midbody and that correct localization of both F-actin and ANLN depends on RhoA activity. Moreover, these observations suggest that localized Rho activity is required to maintain a small pool of F-actin and to recruit ANLN at the secondary ingression sites. Most importantly, they demonstrate that these events are functionally relevant for correct abscission.

CITK controls F-actin, ANLN and CHMP4B localization in secondary ingression sites.

CITK is required to maintain ANLN and active RhoA at the midbody in late cytokinesis (Gai 2011). We therefore asked whether this protein is also necessary for proper cytoskeletal organization at secondary ingression sites. Quantitative analysis of late midbodies showed that both F-actin and ANLN are decreased at secondary sites in CITK-depleted cells, as compared to control (Fig. 2A-C), while their overall abundance in cytoplasm is not significantly different (data not shown). Altered F-actin and ANLN localization is likely produced by increased F-actin depolymerization. Indeed, treatment of cells with the actin-stabilizer Jasplakinolide restored the localization of both F-actin and ANLN (Fig. 2A-C). To assess if control of actin stability is a CITK downstream event relevant for abscission, we studied whether actin stabilization can prevent the cytokinesis failure induced by CITK loss. To this aim, we allowed control and CITK-depleted cells treated with Jasplakinolide, to exit mitosis and quantified the percentage of binucleated cells. Interestingly, Jasplakinolide did not modify binucleation frequency in cells treated with control siRNA, but it reverted to control levels the increased binucleation frequency produced by CITK loss (Fig. 2D).

We previously showed that CITK overexpression leads to midbody hyper-stabilization through RhoA activation, doubling abscission time (Gai et al., 2011). ANLN overexpression induces the same phenotype, acting downstream of RhoA (Gai et al., 2011). Consequently, the percentage of cells in cytokinesis 180 min after nocodazole release was significantly increased by CITK or ANLN overexpression (Gai et al., 2011; Fig. 2E,F). To assess the role of actin dynamics in these phenotypes, we treated telophase-synchronized HeLa cells overexpressing CITK or ANLN with CytoD. Actin depolymerization restored cytokinesis progression to levels of the corresponding controls in both cases (Fig. 2E,F),

Journal of Cell Science • Accepted manuscript

and reverted the increased levels of midbody F-actin produced by CITK overexpression (Fig. S2A). RhoA inhibition through C3-transferase reverts the abscission delay caused by CITK overexpression (Gai et al., 2011). Accordingly, F-actin levels at the midbody of CITK overexpressing cells were restored to normal values by RhoA inhibition (Fig. S2B), confirming that CITK downstream events in late midbodies depend on RhoA activity (Gai et al., 2011).

Altogether, these results indicate that CITK regulates F-actin levels at midbody in late cytokinesis, and support a critical role of actin stability in a CITK-RhoA-Actin-ANLN pathway leading to abscission.

Since the ANLN–septin complex primes the ICB for CHMP4B recruitment at the abscission site (Renshaw et al., 2014), we analyzed whether CHMP4B is disturbed by CITK depletion. In CITK-depleted cells, CHMP4B was correctly associated with the midbody (Fig. 2G), but it did not localize to secondary sites (Fig. 2G). This result suggests that CITK is required for CHMP4B relocalization from midbody to constriction sites.

CITK and ANLN influence actin dynamics at the midbody.

To directly assess whether CITK controls actin dynamics in late cytokinesis, we transfected cells with the live-imaging tracer Lifeact-RFP, which specifically associates with actin filaments (Riedl et al., 2008), and measured its fluorescence intensity at midbody at fixed times after this structure was formed.

In control cells, the Lifeact-RFP signal accumulated at the cleavage furrow during its constriction (Fig. 3A, Movie 3). F-actin accumulation remained well detectable after midbody formation, but it progressively decreased during midbody maturation (Fig. 3B). Nevertheless, in half of cell divisions, after Lifeact-RFP signal reached 20% of the initial intensity, we could detect a late increase of fluorescence just before abscission (*spike*) (Fig. 3B,C,G).

When CITK was depleted, actin disassembly was faster than in control cells (Fig. 3E, Movie 3,4). Indeed, the time required for the reduction of Lifeact-RFP midbody signal from 100% to 20% was significantly decreased (Fig. 3F). Moreover, the frequency of Lifeact spikes was decreased to approximately half of the control (Fig. 3G).

To check if the effect of CITK on actin dynamics is global or local, we biochemically assessed whether CITK depletion alters the ratio between monomeric (G) and filamentous (F) actin, by detergent-based cell fractionation. We could not detect any difference in G/F

Journal of Cell Science • Accepted manuscript

actin ratio in control versus CITK-depleted cells (Fig. S3A,B). This result supports the hypothesis that the effect of CITK on F-actin is temporally and spatially regulated.

When HeLa cells were transfected with a plasmid overexpressing GFP-tagged CITK or ANLN protein, we observed a reduction in the rate of midbody actin decrease (Fig. 4A, Movie 5,6,7). Indeed, in CITK and ANLN overexpressing cells, the time required for Lifeact-RFP midbody signal reduction from 100% to 20% was significantly longer then in control (Fig. 4B). Moreover, there was an increase of divisions in which the Lifeact-RFP fluorescence intensity at the midbody never dropped under 20% of the starting value (Fig. 4C). We observed a decrease of the G/F ratio in CITK transfected cultures (Fig. S3C,D), suggesting that its overexpression exerts a dominant effect on actin polymerization. To directly evaluate whether CITK affects F-actin dynamics at midbody, we resorted to Fluorescence Recovery After Photobleaching (FRAP) of RFP-Actin, performed at midbodies of cells overexpressing CITK or control plasmid (Fig. 4D). CITK increased both RFP-actin recovery half-life and immobile fraction (Fig. 4E,F). These results indicate that CITK controls the disassembly of F-actin at the midbody during late cytokinesis, possibly decreasing F-actin turnover rate, and suggest that ANLN may be relevant for this function.

Conclusion

In this report, we provided evidence that F-actin assembly and disassembly from the ICB in the late cytokinesis stages is finely regulated. Upon complete cleavage furrow ingression, most actin filaments of actomyosin ring disassemble (Dambournet et al., 2011; Guizetti et al., 2011; Saurin et al., 2008; Schiel et al., 2012). However, a small pool of F-actin is maintained at secondary ingression sites, where F-actin colocalizes with ANLN. Moreover, we showed that maintenance of F-actin at secondary sites may be functionally relevant for abscission and that CITK has a fundamental role in this process. When CITK is missing, polymerized actin is prematurely removed and ANLN is not stabilized at the midbody. These events may end up with lack of CHMP4B relocalization at abscission sites and cytokinesis failure. Conversely, when CITK is overexpressed, F-actin disassembly from the midbody is slowed down and abscission is delayed, consistent with previous findings (Gai et al., 2011). Therefore, CITK is required not only for midbody stabilization, as previously demonstrated (Bassi et al., 2013; Gai et al., 2011; Mckenzie et al., 2016), but also for midbody late-stage maturation and final cut. Since CITK does not localize at secondary sites (Hu et al., 2012), while it is necessary to localize F-actin and ANLN, it is

Journal of Cell Science • Accepted manuscript

possible that its catalytic activity may drive post-translational modifications on ANLN and/or on other players, to allow their localization at secondary sites. Further studies will be necessary to investigate these possibilities.

Materials and methods

Cell culture, synchronization and drug treatments

Unmodified HeLa cells were originally obtained from ATCC and a new batch was thawed after 5 passages. All cells are routinely screened for mycoplasma contamination.

HeLa cells were cultured in RPMI medium supplemented with 10% fetal bovine serum (FBS) and 1% penicillin/streptomycin. The HeLa cell line expressing α-tubulin-GFP was maintained in DMEM-GlutaMAX (Invitrogen) supplemented with 10% FBS, 100 Uml^{-1} penicillin, 100 μgml^{-1} streptomycin, 200 μgml^{-1} Geneticin (Sigma, St. Louis, MO, USA) and 0.5 μgml^{-1} puromycin. All cells were cultured in a humidified 5% CO2 incubator at 37°C.

For synchronization, asynchronous cultures were supplemented with 25 ug/ml Aphidicolin (Sigma) and maintained under these conditions for 24 h and then cultured for a further 16 h in fresh complete medium in the presence of 50 ng/ml nocodazole (Sigma) to block cells at prometaphase. Finally, cells were washed three times with fresh medium and allowed to progress through mitosis/cytokinesis for the indicated times.

For time lapse imaging, HeLa cells were synchronized by a double-thymidine block: asynchronous cultures were treated with 2 mM thymidine (Sigma) for 16 h, then released for 4–6 h in fresh complete medium and again blocked for 16 h. Finally, cells were washed twice with fresh medium and allowed to progress through mitosis.

For drug treatments, synchronized HeLa cells were treated with 0.2 0.4 and 1 μM Cytochalasin D (Sigma), 10 nM Jasplakinolide (Merck S.p.A) and Rho inhibitor C3 transferase as described.

Plasmids, siRNAs and cell transfection

In this study, we used a previously validated CITK-siRNA sequence (AUGGAAGGCACUAUUUCUCAA) (Gai et al., 2011) obtained from GE-Healthcare (Dharmacon, Lafayette, CO). The ON-TARGETplus non-targeting siRNA #1 (GE Healthcare, Dharmacon) was used as a negative control for potential off-target effects. The expression construct coding for CITK-GFP was generated by inserting the Myc-CITK

Journal of Cell Science • Accepted manuscript

cDNA into the pm-GFP-N1 plasmid (Clontech, Mountain View, CA) (Gai et al., 2011). The GFP-ANLN construct was kindly provided by A. Piekny (Piekny and Glotzer, 2008).
Transfection was performed with Lipofectamine 2000 (Invitrogen) for siRNA and with TransIT-Lt1 (Mirus) for plasmids, following standard manufacturer protocols.

Antibodies

The following antibodies were used: mouse anti-α-tubulin, 1:1000 (Sigma, Cat. T5168, clone B-5-1-2); rabbit polyclonal anti-ANLN, 1:200 (Bethyl laboratories, a301-406a); rabbit anti-CHMP4B, 1:1000 (provided by Harald Stenmark), rabbit polyclonal anti-actin (Santa Cruz, sc-7210); rabbit anti-GFP, western blot 1:2,000 (Abcam, ab290).

Immunofluorescence

Cells were fixed 4% paraformaldehyde at room temperature for 10 min for ANLN and actin staining or with methanol at -20°C for 10 min for CHMP4B staining. In all cases, cells were permeabilized in 0.1% Triton X 100 in PBS for 10 minutes, saturated in 5% BSA in PBS for 30 minutes and incubated with primary antibody for 45 min at room temperature. Primary antibodies were detected with anti–rabbit or anti–mouse Alexa Fluor 488/568/647 (Molecular Probes, Invitrogen), used at 1:1000 dilution for 30 min. For F-actin staining, Acti-stain 488 phalloidin (Cytoskeleton Denver, CO) was used in accordance with the manufacturer's instructions. Counterstaining was performed with the DNA dye DAPI (Sigma) at 0.5 μg/ml for 1 minute.

Western Blot and G/F-actin quantification

Western blot was performed following standard protocols. For G/F-actin quantification, unsynchronized HeLa cells were firstly lysed in a solution containing 30% glycerol and 1% Triton X-100, buffered with PIPES, EGTA and $MgSO_4$, and the lysate was considered corresponding to cytosolic fractions. The resulting pellets were then lysed again in a solution containing 1.5% SDS and 25 mM Tris-HCl pH 6.8 at 95°C; the resulting lysate was considered corresponding to cytoskeletal elements.

Microscopy

Imaging was performed using a Leica TCS SP5 confocal system (Leica Microsystems) equipped with a 405 nm diode, an argon ion, a 561 nm DPSS and a HeNe 633 nm lasers. Fixed cells were imaged using a HCX PL APO 63x/1.4 NA oil immersion objective. For live imaging, time lapses were recorded overnight with an interval of 5 minutes using a 40X

Journal of Cell Science • Accepted manuscript

PlanApo N.A. 1.4 oil immersion objective on the cells kept in the microscope incubator at 37°C and 5% CO2.

FRAP experiments were performed on midbodies of constant size using 100% transmission of 568 nm laser for photobleaching. Recovery kinetics were then measured and, after background subtraction, were normalized to pre-bleach frames.

Super resolution images were obtained using a Leica SP8 confocal system with HyVolution 2 (Leica Microsystems) equipped with an argon ion, a 561 nm DPSS and a HeNe 633 nm lasers. Fixed cells were imaged using a HCX PL APO 63x/1.4 NA oil immersion objective. Series of x-y-z images (typically 0.04*0.04*0.106 μm^3 voxel size) were collected.

Image analysis

Lifeact RFP expressing HeLa cells were imaged from anaphase to abscission using a Leica SP5 confocal laser-scanning microscope, with red fluorescence and DIC frames acquired every 5 minutes. We acquired images with low laser power and frame rate in order to avoid bleaching. The intensity of Lifeact fluorescence at the midbody was evaluated with ImageJ in an area of fixed surface manually imposed on the midbody ring, identified by the DIC image. The completion of cleavage furrow ingression was considered as time 0. The resulting intensity values were corrected for background by subtracting the average fluorescence intensity of 3 points of identical surface measured in areas devoid of cells, and then normalized to the initial value at time 0.

To determine the decrease of midbody Lifeact fluorescence intensity, for each graph we considered the first occurrence in which the signal dropped below 20% of the initial amount for at least two successive frames (i.e., for at least 5 minutes). We identified as a second actin spike an increase of the Lifeact intensity signal higher than 20%, after the initial drop and persisting for at least two consecutive frames.

Quantitative analysis of protein localization was obtained using ImageJ (Rueden et al., 2017; Schindelin et al., 2012). For ANLN, F-actin and CHMP4B an intensity profile was generated along the intercellular bridge; the ratio between fluorescence intensity at the secondary sites and the midbody was calculated; finally, a threshold was set in order to discriminate among positive and negative secondary ingression sites. Analysis requiring manual counting were performed on blinded samples. To determine F-actin intensity at the intercellular bridge (ICB), F-actin mean fluorescence intensity of a fixed area corresponding to the ICB was measured and normalized to the F-actin mean fluorescence

Journal of Cell Science • Accepted manuscript

intensity of the total cell. For analysis of F-actin localization in C3 treated synchronized cells, an intensity profile was created along the intercellular bridge and the distance between the lower intensity point of tubulin at the midbody and the lower intensity point of tubulin at the secondary ingression site (D1) was measured. We then measured the distance between the midbody and the higher intensity point of F-actin (D2). We finally calculated the ratio between D2 and D1.

Statistics

Statistical analyses were performed using Microsoft Office Excel or Graphpad (GraphPad Software). All the numbers represented by histograms were obtained by averaging all the data points contained in the replicas (with a comparable number of points per each replica). Unpaired Student's t test and Chi-square were used for p values determination as indicated.

Competing interests

The authors declare that they have no conflict of interest.

Funding

This work was supported by Associazione Italiana per la Ricerca sul Cancro (AIRC) through grant IG17527, by Telethon Foundation through grant n. GGP12095 and n. GGP13081 and by 'Consiglio Nazionale delle Ricerche' through the EPIGEN project to F.D.C.

Journal of Cell Science • Accepted manuscript

References

Agromayor, M. and Martin-Serrano, J. (2013). Knowing when to cut and run: Mechanisms that control cytokinetic abscission. *Trends Cell Biol.* **23**, 433–441.

Bassi, Z. I., Verbrugghe, K. J., Capalbo, L., Gregory, S., Montembault, E., Glover, D. M. and D'Avino, P. P. (2011). Sticky/Citron kinase maintains proper RhoA localization at the cleavage site during cytokinesis. *J. Cell Biol.* **195**, 595–603.

Bassi, Z. I., Audusseau, M., Riparbelli, M. G., Callaini, G. and D'Avino, P. P. (2013). Citron kinase controls a molecular network required for midbody formation in cytokinesis. *Proc. Natl. Acad. Sci. U. S. A.* **110**, 9782–7.

Dambournet, D., Machicoane, M., Chesneau, L., Sachse, M., Rocancourt, M., El Marjou, A., Formstecher, E., Salomon, R., Goud, B. and Echard, A. (2011). Rab35 GTPase and OCRL phosphatase remodel lipids and F-actin for successful cytokinesis. *Nat. Cell Biol.* **13**, 981–8.

Eggert, U. S., Mitchison, T. J. and Field, C. M. (2006). Animal cytokinesis: from parts list to mechanisms. *Annu. Rev. Biochem.* **75**, 543–66.

El Amine, N., Kechad, A., Jananji, S. and Hickson, G. R. X. (2013). Opposing actions of septins and Sticky on Anillin promote the transition from contractile to midbody ring. *J. Cell Biol.* **203**, 487–504.

Elia, N., Sougrat, R., Spurlin, T. A., Hurley, J. H. and Lippincott-schwartz, J. Dynamics of endosomal sorting complex required for transport (ESCRT) machinery during cytokinesis and its role in abscission.

Elia, N., Sougrat, R., Spurlin, T. A., Hurley, J. H. and Lippincott-Schwartz, J. (2011). Dynamics of endosomal sorting complex required for transport (ESCRT) machinery during cytokinesis and its role in abscission. *Proc. Natl. Acad. Sci.* **108**, 4846–4851.

Gai, M., Camera, P., Dema, A., Bianchi, F., Berto, G., Scarpa, E., Germena, G. and Di Cunto, F. (2011a). Citron kinase controls abscission through RhoA and anillin. *Mol. Biol. Cell* **22**, 3768–78.

Gai, M., Camera, P., Dema, A., Bianchi, F., Berto, G., Scarpa, E., Germena, G. and Di Cunto, F. (2011b). Citron kinase controls abscission through RhoA and anillin. *Mol. Biol. Cell* **22**,.

Guizetti, J., Schermelleh, L., Mäntler, J., Maar, S., Poser, I., Leonhardt, H., Müller-Reichert, T., Gerlich, D. W., Barr, F. A., Gruneberg, U., et al. (2011). Cortical constriction during abscission involves helices of ESCRT-III-dependent filaments. *Science* **331**, 1616–20.

Hu, C. C.-K. C.-K., Coughlin, M., Mitchison, T. J. and Doxsey, S. (2012). Midbody assembly and its regulation during cytokinesis. *Mol. Biol. Cell* **23**, 1024–1034.

McKenzie, C., Bassi, Z. I., Debski, J., Gottardo, M., Callaini, G., Dadlez, M. M. and D'Avino, P. P. (2016). Cross-regulation between Aurora B and Citron kinase controls midbody architecture in cytokinesis. *Open Biol.* **6**, 160019.

Mierzwa, B. and Gerlich, D. W. (2014). Cytokinetic Abscission: Molecular Mechanisms and Temporal Control. *Dev. Cell* **31**, 525–538.

Piekny, A. J. and Glotzer, M. (2008). Anillin Is a Scaffold Protein That Links RhoA, Actin, and Myosin during Cytokinesis. *Curr. Biol.* **18**, 30–36.

Pollard, T. D. (2010). Mechanics of cytokinesis in eukaryotes. *Curr. Opin. Cell Biol.* **22**, 50–6.

Renshaw, M. J., Liu, J., Lavoie, B. D. and Wilde, A. (2014). Anillin-dependent organization of septin filaments promotes intercellular bridge elongation and Chmp4B targeting to the abscission site. *Open Biol.* **4**, 130190.

Riedl, J., Crevenna, A. H., Kessenbrock, K., Yu, J. H., Neukirchen, D., Bista, M.,

Journal of Cell Science • Accepted manuscript

Bradke, F., Jenne, D., Holak, T. A., Werb, Z., et al. (2008). Lifeact: a versatile marker to visualize F-actin. *Nat. Methods* **5**, 605–7.

Rueden, C. T., Schindelin, J., Hiner, M. C., DeZonia, B. E., Walter, A. E., Arena, E. T. and Eliceiri, K. W. (2017). ImageJ2: ImageJ for the next generation of scientific image data. *BMC Bioinformatics* **18**,.

Saurin, A. T., Durgan, J., Cameron, A. J., Faisal, A., Marber, M. S. and Parker, P. J. (2008). The regulated assembly of a PKCepsilon complex controls the completion of cytokinesis. *Nat. Cell Biol.* **10**, 891–901.

Schiel, J. a., Park, K., Morphew, M. K., Reid, E., Hoenger, a. and Prekeris, R. (2011). Endocytic membrane fusion and buckling-induced microtubule severing mediate cell abscission. *J. Cell Sci.* **124**, 1769–1769.

Schiel, J. A., Simon, G. C., Zaharris, C., Weisz, J., Castle, D., Wu, C. C. and Prekeris, R. (2012). FIP3-endosome-dependent formation of the secondary ingression mediates ESCRT-III recruitment during cytokinesis. *Nat. Cell Biol.* **14**, 1068–78.

Schindelin, J., Arganda-Carreras, I., Frise, E., Kaynig, V., Longair, M., Pietzsch, T., Preibisch, S., Rueden, C., Saalfeld, S., Schmid, B., et al. (2012). Fiji: An open-source platform for biological-image analysis. *Nat. Methods* **9**, 676–682.

Watanabe, S., De Zan, T., Ishizaki, T. and Narumiya, S. (2013). Citron kinase mediates transition from constriction to abscission through its coiled-coil domain. *J. Cell Sci.* **126**, 1773–84.

Journal of Cell Science • Accepted manuscript

Figures

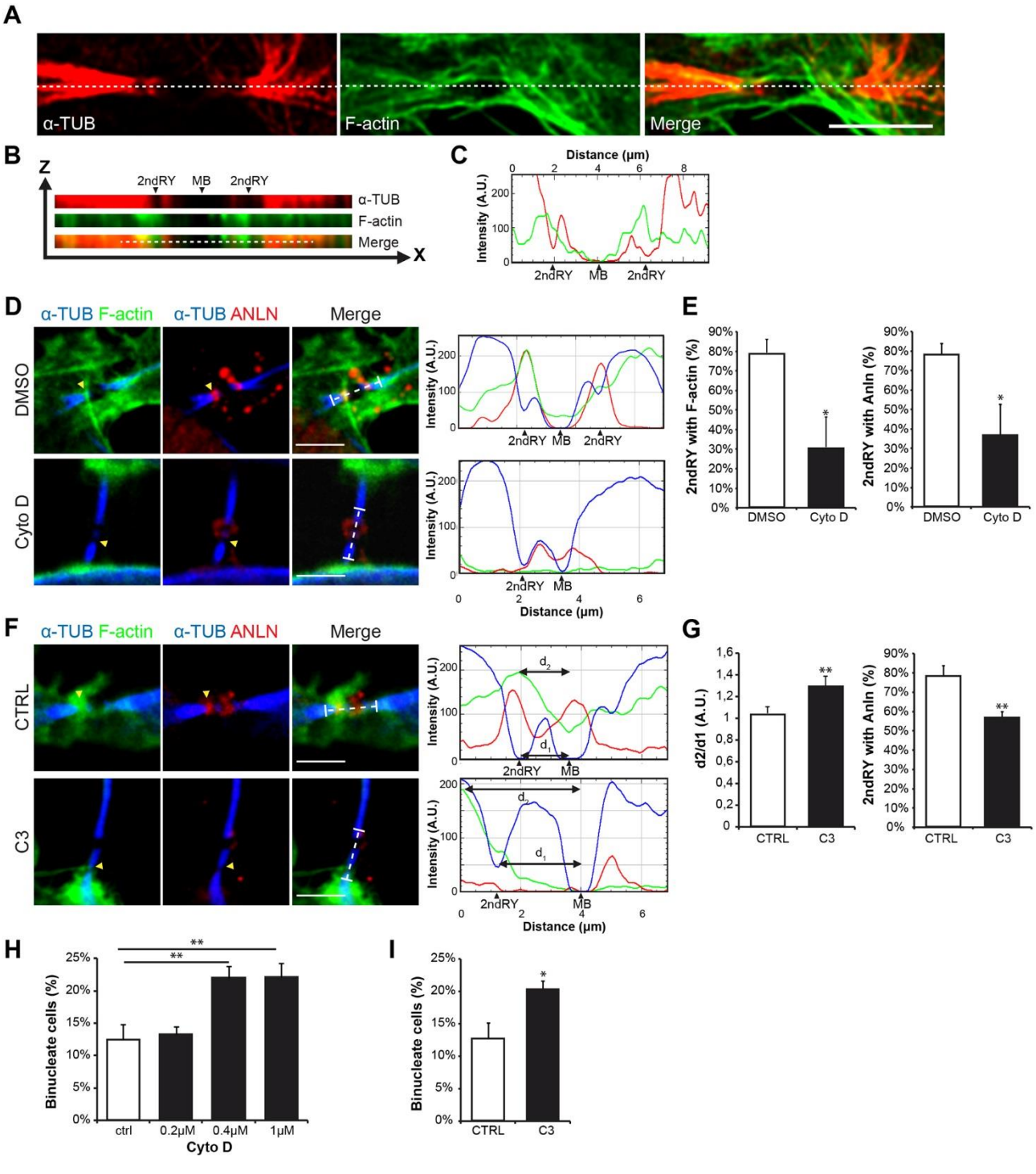

Journal of Cell Science • Accepted manuscript

Figure 1. F-actin localizes at secondary ingression sites and is required for abscission. (A) ICB of HeLa cells stained for α-tubulin and F-actin. Images were acquired using super-resolution confocal microscopy. Dotted lines indicate the plane of cross section (XZ) shown in B. (C) Intensity profile, plotted for the two channels along the ICB (dotted line). (D-G) HeLa cells were synchronized in late cytokinesis, treated for 60 min with 0.4 μM CytoD or DMSO (D-E) and with C3 or control solution (F-G) and immunostained for α-tubulin, ANLN and F-actin. Images were acquired using confocal microscopy. *Left panel:* yellow arrowheads indicate secondary ingression sites. *Right panel:* intensity profile plotted for the three channels along the ICB (dotted line). (E) Quantification of the percentage of secondary ingression sites positive for F-actin and ANLN, in midbodies of cells treated as in D ($n > 50$, N=3). (G) Quantification of F-actin distribution (left histogram) and of the percentage of secondary ingression sites positive for ANLN, in midbodies of cells treated as in F. ($n > 50$, N=3). (H-I) Cell were synchronized as in D-G, treated either with increasing concentration of CytoD (H) or with C3 (I) and fixed 180 min after drugs addition. The percentage of binucleated cells was determined by DAPI and α-tubulin staining and fluorescence microscopy ($n > 300$ cells, N=3). Scale bars, 5 μm. MB = midbody; 2ndRY = secondary ingression sites.

Data shown in histograms are means ± s.e.m. Statistical significance was assessed using a two tails Student T-test. *** $p < 0.001$ ** $p < 0.01$ * $p < 0.05$.

Journal of Cell Science • Accepted manuscript

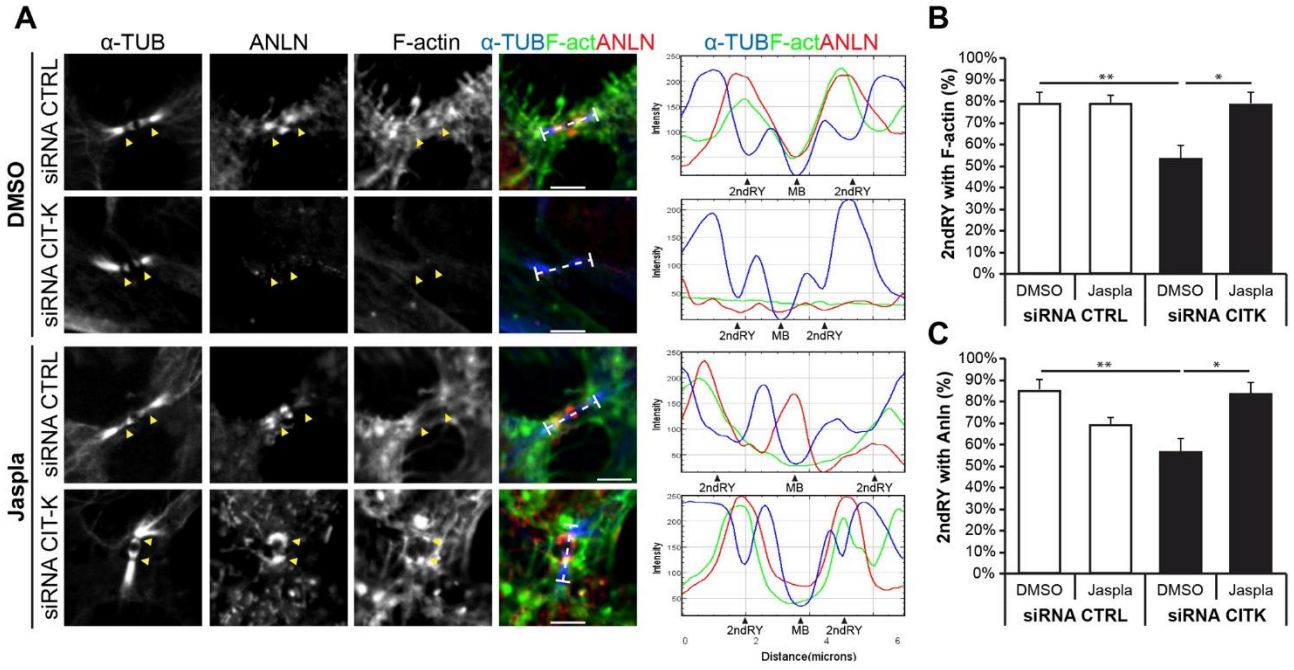

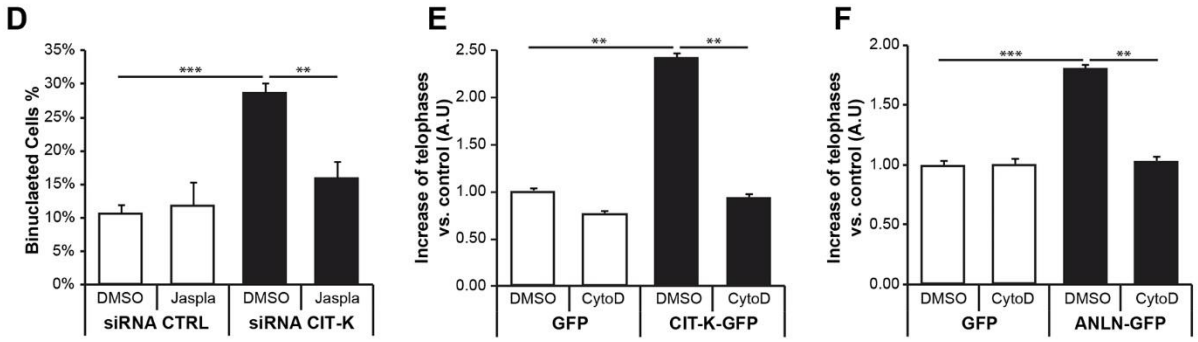

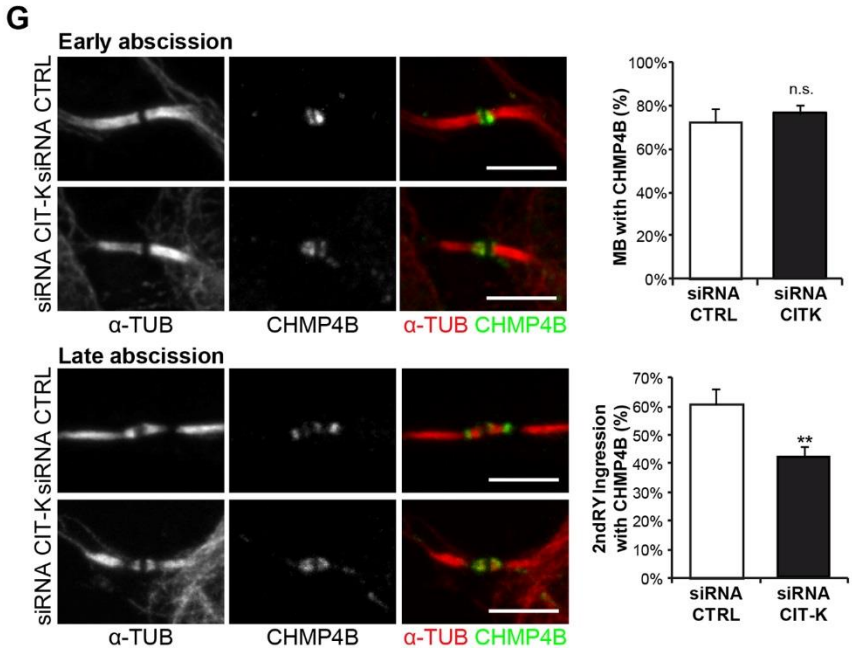

Journal of Cell Science • Accepted manuscript

Figure 2. CITK is required for F-actin, ANLN and CHMP4B localization at secondary ingression sites. (A) HeLa cells treated with control or CITK siRNAs were synchronized in late cytokinesis, treated with 10 nM Jasplakinolide or DMSO for 60 min and immunostained for α-tubulin, ANLN and F-actin. Images were acquired using confocal microscopy. *Left panel:* yellow arrowheads indicate secondary ingression sites. *Right panel:* intensity profile plotted for the three channels along the ICB (dotted line). (B-C) Quantification of the percentage of secondary ingression sites positive for F-actin (B) and ANLN (C) in midbodies of cells treated as in A (n > 50, N=3). Scale bars, 5 μm. (D) HeLa cells, transfected with control or CITK siRNAs, were treated as in A and fixed after 180 min following Jasplakinolide addition. The percentage of binucleated cells was determined by DAPI and α-tubulin staining followed by fluorescence microscopy (n > 300 cells, N=3). (E-F) Hela cells were transfected with GFP, CITK-GFP or ANLN-GFP, synchronized as in A and treated with 1 μM CytoD or DMSO, fixed after 60 min and stained with DAPI and α-tubulin. Abscission delay was evaluated measuring the relative increase of telophases in cells overexpressing CITK and ANLN, versus control cells (n > 300, N=5). (G) HeLa cells treated as in A were immunostained for α-tubulin and CHMP4B. Images were acquired using confocal microscopy. Cells in telophase were considered early or late abscissions based on the presence of secondary ingression sites. Percentage of either midbodies (*upper panel*) or secondary ingression sites (*lower panel*) positive for CHMP4B was quantified. (n > 50, N=4). Scale bars, 5 μm. MB = midbody; 2ndRY = secondary ingression sites.

Data shown in histograms are means ± s.e.m. Statistical significance was assessed using a two tails Student's T-test. *** $p < 0.001$ ** $p < 0.01$ * $p < 0.05$ n.s. not significant.

Journal of Cell Science • Accepted manuscript

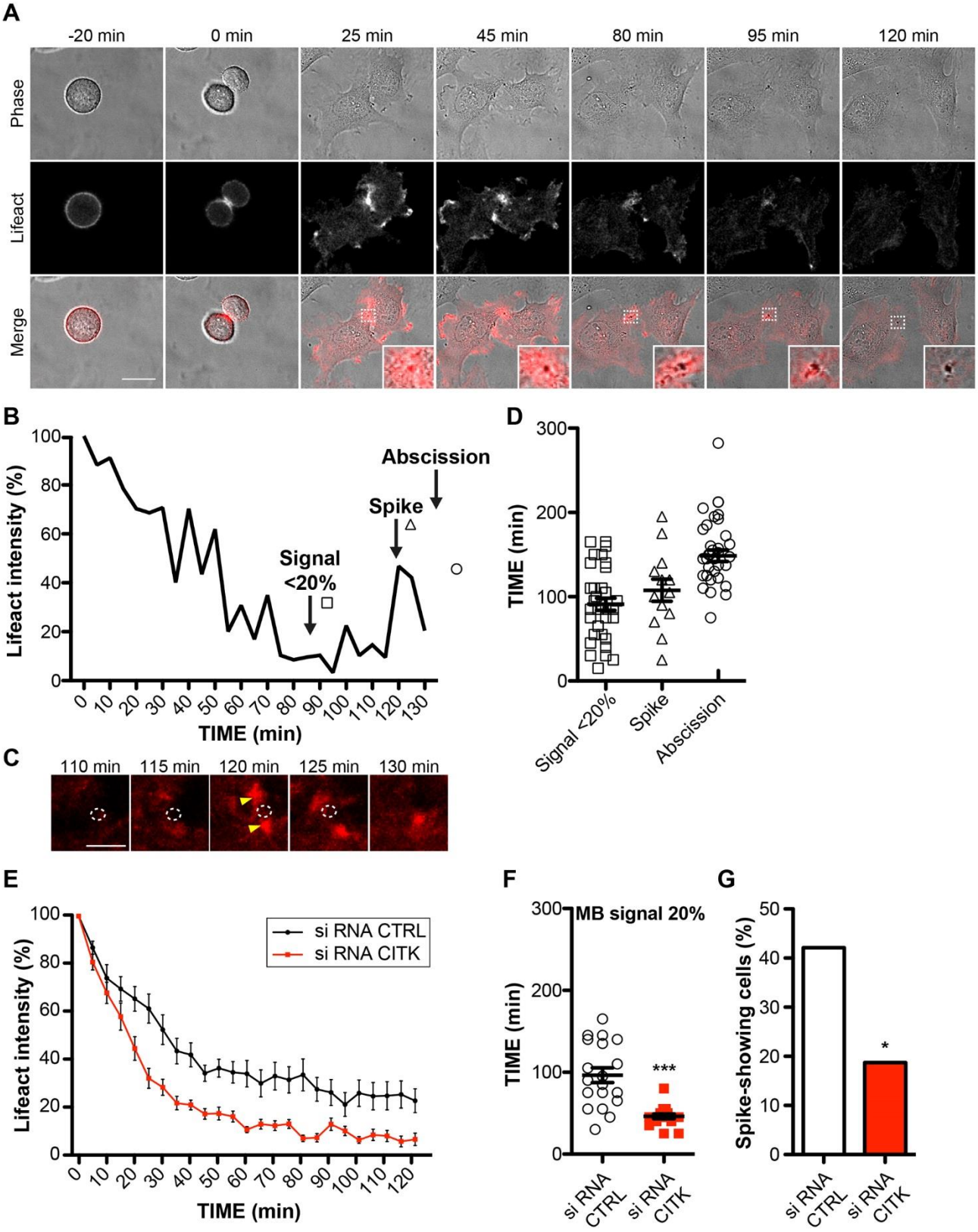

Journal of Cell Science • Accepted manuscript

Figure 3. CITK depletion speeds up F-actin disassembly from the midbody. (A) Selected frames from time-lapse imaging experiments of HeLa cells undergoing cytokinesis (Movies 3-4). HeLa cells were transfected with Lifeact-RFP and observed 30 h post-transfection. Scale bars, 20 µm. (B-G) Fluorescence intensity of Lifeact-RFP at the midbody was analyzed in control and CITK-depleted HeLa cells every 5 minutes for 120 min after cleavage furrow ingression (time 0). Lifeact-RFP intensity at time 0 was set as 100%. (B) Example of intensity profile of midbody Lifeact-RFP from completion of cleavage furrow ingression to abscission. F-actin disassembly *('MB signal <20%')*, second spike of actin polymerization (*'spike'*) and abscission are indicated. (C) Zoomed in images from time-lapse experiment showing a spike (yellow arrowheads) in actin polymerization at the midbody (white circle). (D) Distribution and average of times required in control cells for F-actin disassembly *('MB signal <20%')*, second spike of actin polymerization (*'spike'*) and abscission. (E) Normalized values of Lifeact intensity at the midbody in control and CITK-depleted HeLa cells were averaged and plotted. (F) Time for F-actin disassembly was measured in control and CITK-depleted HeLa cells.

Data shown in histograms are means ± s.e.m. Statistical significance was assessed using a two tails Student's T-test. *** $p < 0.001$. * $p < 0.05$. $n > 10$ cells in all the analyzed cases. (G) Percentage of cytokinesis with the second spike of actin polymerization.

Statistical significance was assessed using a Chi-square test. * $p < 0.05$ ($n > 10$, N=3).

Journal of Cell Science • Accepted manuscript

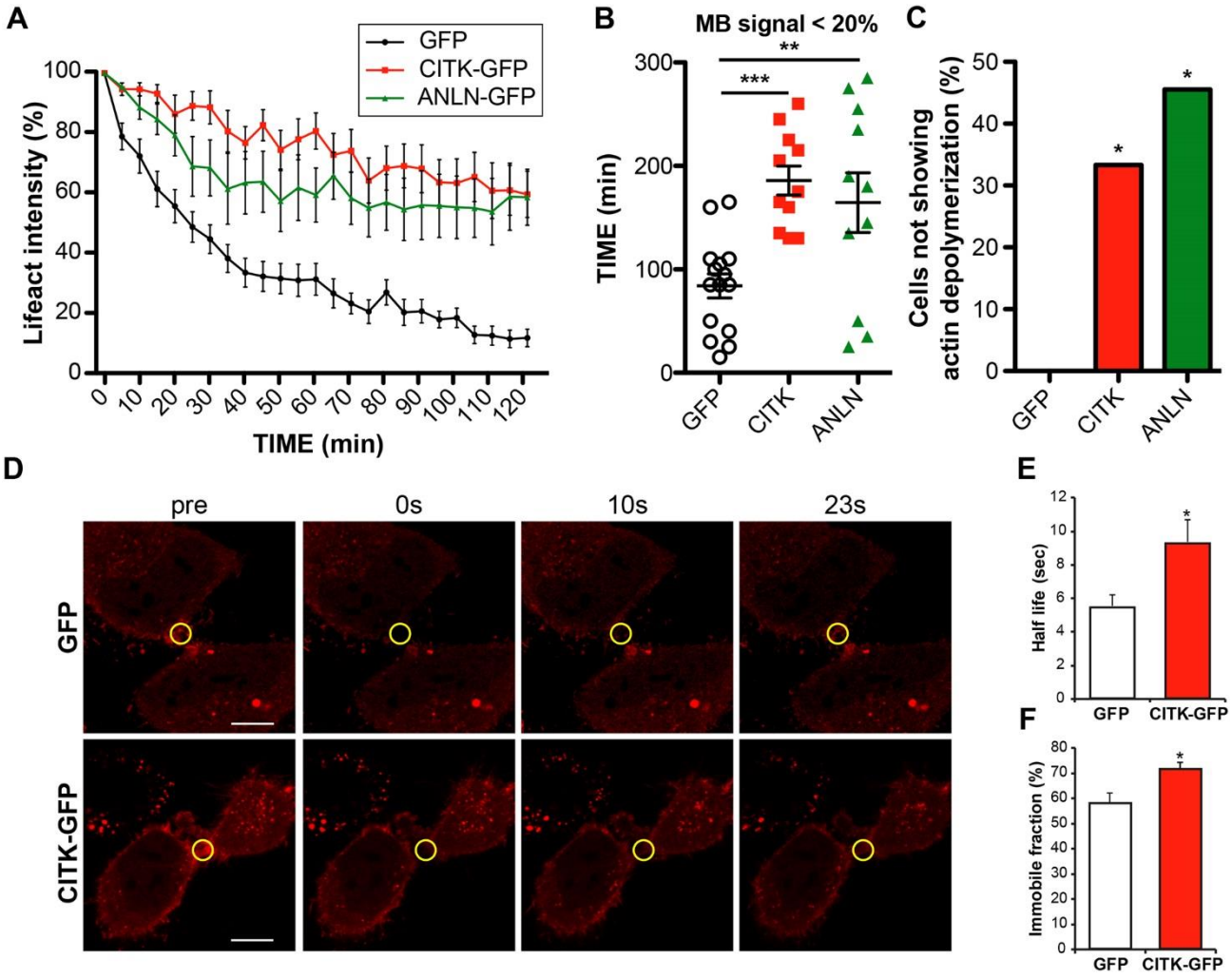

Figure 4. CITK and ANLN overexpression stabilizes F-actin in the midbody. HeLa cells were transfected with Lifeact-RFP and observed 30 h post-transfection. (A) Fluorescence intensity of Lifeact-RFP at the midbody was analysed in HeLa cells expressing either GFP, CITK-GFP or ANLN-GFP (Movies 5-6-7). Time 0 was set when cleavage furrow ingression was completed; Lifeact-RFP intensity of time 0 was set 100%. (B) Time for F-actin intensity decrease from 100 to 20% *('MB signal <20%')* was calculated in cells treated as in A. (C) Quantification of the percentage of cytokinesis without actin depolymerization from the midbody in cells treated as in A.

Statistical significance was assessed using a Chi-square test. * $p < 0.05$ ($n > 10$, N=3).

(D-F) Actin dynamics were analyzed by FRAP analysis in Hela cells transfected with RFP-actin together with either CITK-GFP or GFP. (D) Selected frames of FRAP experiments before (*pre*) and after bleaching and throughout the recovery. Yellow circle indicates the

Journal of Cell Science • Accepted manuscript

ROI used for FRAP analysis. (E-F) Half life and immobile fraction of actin in the midbody were measured (n > 10, N=3).

Data shown in histograms are means ± s.e.m. Statistical significance was assessed using a two tails Student's T-test. *** $p < 0.001$ ** $p < 0.01$ * $p < 0.05$.

Journal of Cell Science • Accepted manuscript

Supplemental Figures

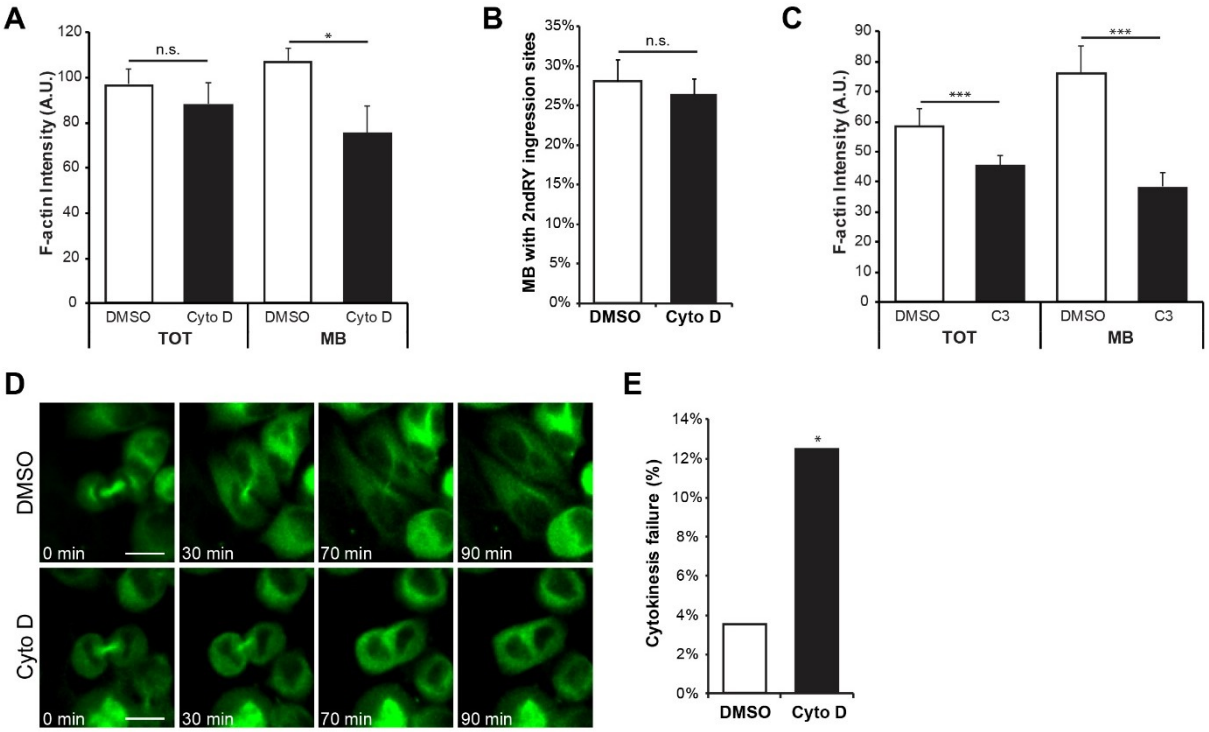

Supplemental Figure 1. Effects of F-actin depolymerisation in late cytokinesis. (A) HeLa cells were synchronized in late cytokinesis, treated with 0,4 μM Cytochalasin D (CytoD) or DMSO for 60 min and immunostained for α-tubulin and F-actin. Total cell (*TOT*) or midbody (*MB*) F-actin intensity was quantified. (B) Percentage of midbodies with secondary (*2ndRY*) ingression sites in cell treated as in (A) (n > 30) (C) HeLa cells were synchronized in late cytokinesis, treated with the RhoA inhibitor C3-transferase or control solution for 60 min and immunostained for α-tubulin and F-actin. Total cell (*TOT*) or midbody (*MB*) F-actin intensity was quantified (n > 30, 3 independent experiments).

Data shown in histograms are means ± s.e.m. Statistical significance was assessed using a two tails Student T-test. * $p < 0.05$. *** $p < 0.001$.

(D) Time-lapse imaging of α-tubulin-GFP-expressing HeLa cells was started after Cytochalasin D addition. Scale bars, 20μm. For full movie, see Movies 1-2. (C) Quantification of cytokinesis failures of cells treated as in (D), only cells with complete cleavage furrow ingression at the time of Cytochalasin D addition were analyzed.

Data shown in histogram are the percentage of cytokinesis failures on the total number of cytokinesis analyzed. Statistical significance was assessed using a Chi-square test. * $p < 0.05$ (n > 60).

Journal of Cell Science • Supplementary information

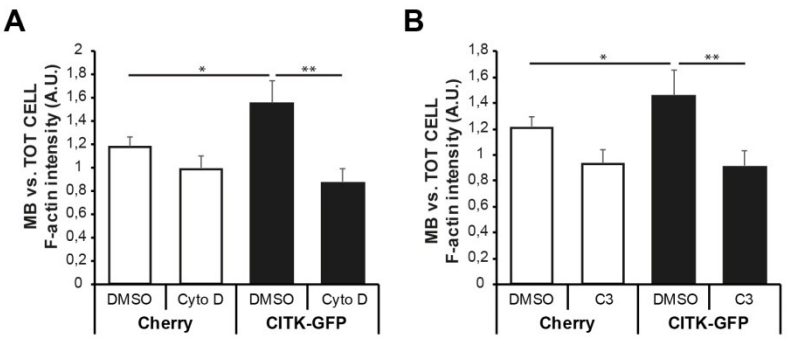

Supplemental Figure 2. Cytochalasin D treatment and RhoA inhibition could revert actin stabilization at the midbody caused by CITK overexpression. HeLa cells expressing either GFP or CITK-GFP were synchronized in late cytokinesis, treated with 0.4 μM Cytochalasin D or DMSO (A) and with RhoA inhibitor C3-transferase or control solution (B) for 60 min and immunostained for α-tubulin and F-actin. Midbody (*MB*) versus total cell (*TOT*) F-actin intensity was quantified (n > 30, 6 independent experiments).
Data shown in histograms are means ± s.e.m. Statistical significance was assessed using a two tails Student T-test. * $p < 0.05$. ** $p < 0.01$.

Journal of Cell Science • Supplementary information

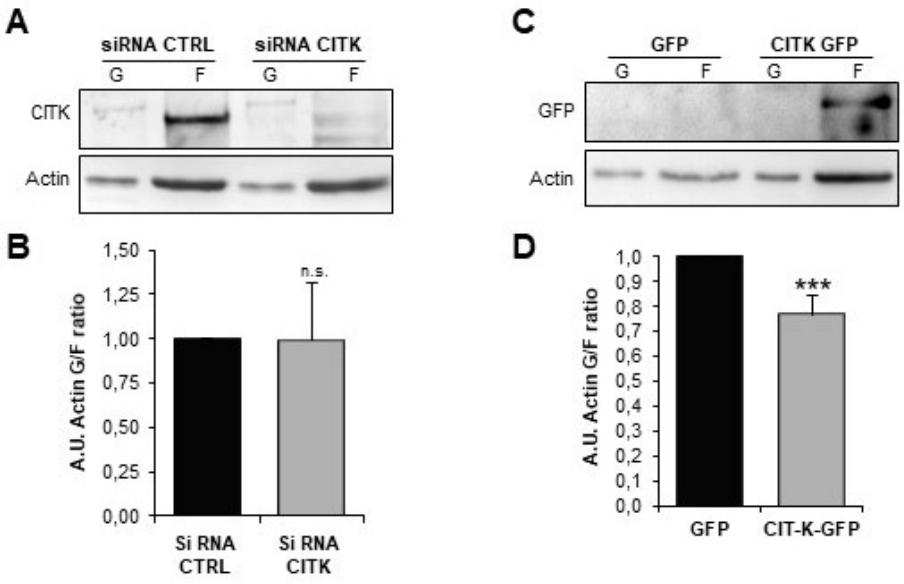

Supplemental Figure 3. CITK overexpression increases actin polymerization. G/F actin fractionation was performed on HeLa cells treated with control or CITK siRNAs (A, B) and on GFP or CITK-GFP expressing HeLa cells (C, D) and the resulting lysates were run on western blot, then G/F actin ratio was calculated (n =4). Data shown in histograms are means ± s.e.m. Statistical significance was assessed using a two tailed Student T-test. *** $P < 0.001$ n.s. not significant.

Journal of Cell Science • Supplementary information

Movies

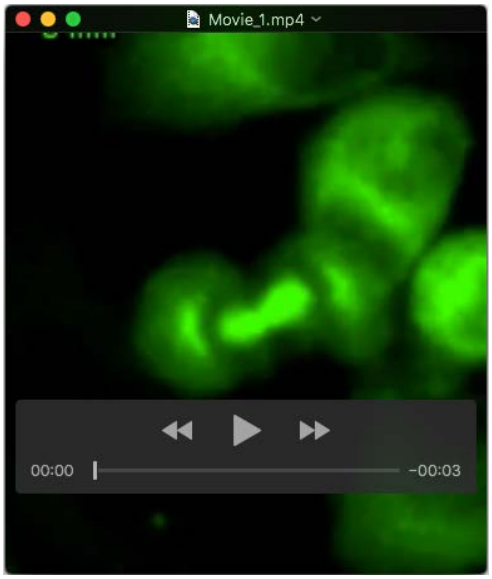

Movie 1. Time-lapse of HeLa cells stably expressing TUB-GFP synchronized and treated with DMSO after midbody formation.

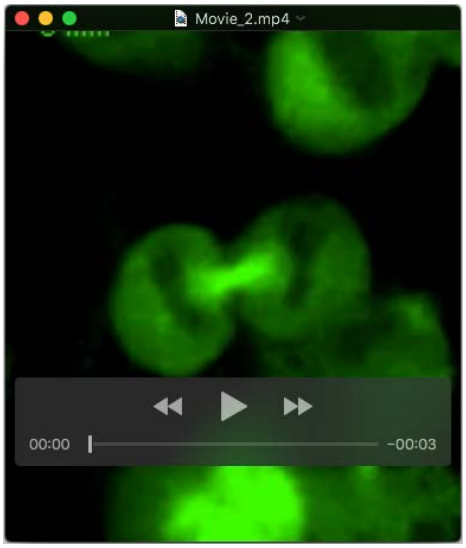

Movie 2. Time-lapse of HeLa cells stably expressing TUB-GFP synchronized and treated with 1uM Cytochalasin D after midbody formation.

Journal of Cell Science • Supplementary information

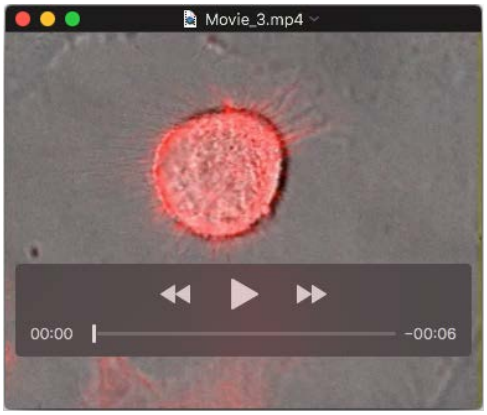

Movie 3. Time-lapse of HeLa cells transfected with Lifeact-RFP treated with control siRNA.

Movie 4. Time-lapse of HeLa cells transfected with Lifeact-RFP treated with CIT-K siRNA.

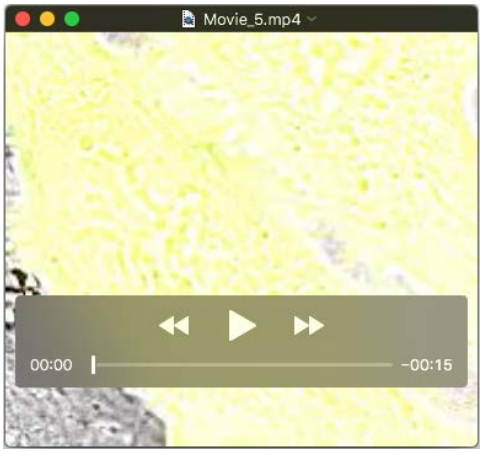

Movie 5. Time-lapse of HeLa cells transfected with Lifeact-RFP expressing GFP.

Journal of Cell Science • Supplementary information

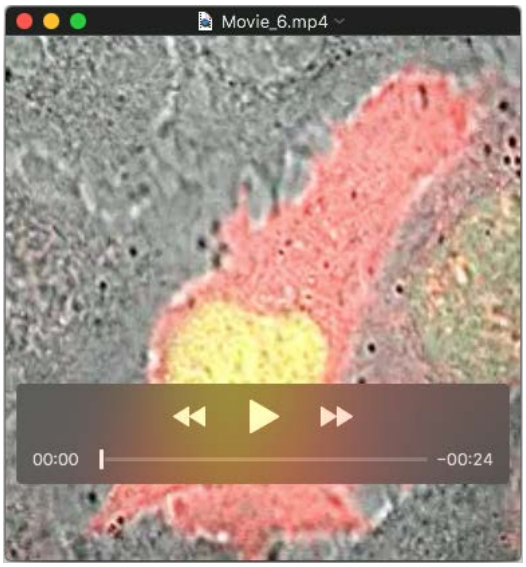

Movie 6. Time-lapse of HeLa cells transfected with Lifeact-RFP expressing CITK-GFP.

Movie 7. Time-lapse of HeLa cells transfected with Lifeact-RFP expressing ANLN-GFP.

Journal of Cell Science • Supplementary information